Water Droplet Breakup In High Speed Airstreams

by

Arthur A. Ranger*
Aerospace Sciences Laboratory, Purdue University
Lafayette, Indiana 47907

and

J. A. Nicholls†
Gas Dynamics Laboratories, The University of Michigan
Ann Arbor, Michigan 48104

ABSTRACT

This paper presents new experimental data on the shattering of water droplets in supersonic airstreams. Water droplets, created by using a vibrating capillary technique, were introduced into the test section of a shock tube where they interacted with the convective flow established by the passage of an incident shock wave. A series of experiments are described in which the initial droplet diameter, convective flow Mach number, and airstream density were systematically varied to obtain results covering a wide range of aerodynamic conditions. High speed photographic techniques utilizing both image converter and rotating drum type cameras were used to photograph the disintegration process in its entirety. The data obtained from the photographs is presented and interpreted to yield such quantities of interest as the breakup time and distance, the drag coefficient, the secondary droplet (or residue) size, and etc. Correlations are presented which indicate that the results can be analyzed in terms of a non-dimensional breakup time.

---

*Assistant Professor, School of Aeronautics, Astronautics, and Engineering Sciences.

†Professor, Department of Aerospace Engineering.

The work reported here was conducted under NASA Contract NASr 54(07).

1. INTRODUCTION

The supersonic flight of a vehicle through the atmosphere is characterized by the production of a high speed flow field in the region of separation between the vehicle's surface and its bow shock wave. The physical and geometrical properties of this flow field are determined primarily by the shape of the vehicle and by its flight Mach number and altitude. Should the vehicle encounter a rain storm or a cloud, the droplets would be exposed to the flow field and perhaps shattered by the aerodynamic forces before striking and possibly damaging the surface of the vehicle. Thus the shattering phenomenon can play an important role in the alleviation of rain erosion problems connected with high speed flight in the atmosphere.

Aside from the work of the authors[1,2,3], the most recent studies conducted on the aerodynamic breakup of liquid drops have been reported by Engel[4], Nicholson[5], and Reinecke[6]; all of whom employed shock tubes to generate the test conditions for their experiments. For an extensive survey of the literature on this subject, however, one should refer to Refs. 1 and 3. In the paragraphs which follow a series of experiments are described and the data presented and analyzed to give new results for the breakup problem under severe aerodynamic conditions.

2. EXPERIMENTAL ARRANGEMENT

The water droplet shattering experiments were conducted in a pressure driven shock tube facility especially designed for this purpose. A detailed description of the entire facility is contained in Ref. 3. The lengths of the driver and the driven sections of the tube were chosen to insure the availability of an adequate testing time over a wide range of operational conditions. All of the testing was confined to the convective flow region between the incident shock front and the interface separating the driver from the driven gas. Both high pressure nitrogen and helium were used as driver gases to create normal shock waves in air having Mach numbers as high as $M_s = 5.7$. The initial air pressure in the driven section, corresponding to a desired pressure altitude, was pre-set and controlled through the use of a vacuum system and a bleed valve.

The test section of the shock tube facility is shown in Fig. 1 where elements of the droplet generator and the photographic system are also visible. The shock waves produced in the tube propagate from the right toward the left through the windowed section where the interaction phenomena between the shock induced convective flow field and the droplets were photographed. The evenly spaced vertical lines appearing along the window are fiducial markers to aid in the data reduction from the photographs.

Water droplets of various sizes were created for the experiments by using a vibrating capillary technique. A detailed account of droplet production using this method is contained in Ref. 3 and in a paper by Dabora[7]. Once generated, the stream of droplets were allowed to fall vertically through the test section and into a collection container fastened, as shown in Fig. 1, to the bottom of the shock tube directly beneath the droplet generator. The droplets formed in this manner were highly stable and reproducible and, hence, ideal for such experiments.

Both an image converter and a rotating drum camera photographic system were employed to obtain a pictorial record of the breakup phenomena. The image converter camera, shown in Fig. 1, was used to take a series of individual time-resolved shadow photographs. The droplets were back-lighted with a high intensity light source and the operation of the image tube was synchronized with the passage of the shock wave through the test section.

Streak photographs of the breakup process were obtained by using a rotating drum camera as shown in Fig. 2. As indicated in the diagram, the streak photographs of a single disintegrating droplet were taken by placing a narrow horizontal slit in the collimated light path. Again the droplets were illuminated by a bright light source which was synchronized to operate when the shock wave passed by.

3. EXPERIMENTAL RESULTS

A large number of experiments were conducted, with both large and small water droplets under a variety of aerodynamic conditions, in order to collect a sufficient amount of data from which useful correlations could be made. The image converter pictures provided a wealth of information with regard to the details of the shattering; e.g. the droplet deformation, the breakup mechanism, the droplet displacement, the time required for a droplet to be completely destroyed, etc. On the other hand, the rotating drum camera captured the entire breakup process in one continuous writing from the moment the shock first made contact with a drop until it had been totally disintegrated.

Many of the details of the shattering process can be observed in the photographs which appear in Fig. 3. These are image converter pictures taken of a stream of 750μ water droplets interacting with the convective flow induced by a Mach two incident shock wave. The incident shock wave moves from the left toward the right across the stream of droplets setting in motion a flow having a convective velocity (U_2) approximately equal to 1400 ft/sec, a convective Mach number (M_2) approximately equal to unity, and a dynamic pressure (q_2) equal to 50 psia. The initial pressure and temperature in the test section were, respectively, 1 atmos. and 75°F. The time in micro-seconds, indicated beneath each photograph, is a measure of the time elapsed between the moment of initial impact with the shock front and the instant at which the picture was taken.

These photographs clearly show the effects of both the pressure and the viscous forces of the airstream on the droplets. One observes that the distributed pressure forces rapidly push or squash the droplet mass into a lenticular shape having a diameter several times that of an undisturbed droplet. Then, while the pressure forces are deforming the drop, the viscous forces exerted by the airstream on the droplet surface apparently erode the liquid surface away through what appears to be a boundary layer stripping mechanism. This material which is stripped away from the surface forms a wake of micro-mist behind the drop as is evident in the photographs.

Under supersonic convective flow conditions the flow field of a disintegrating drop is characterized by the presence of a bow shock wave as seen in Fig. 4. For this particular experiment, the initial pressure and temperature of the air in the test section were the same as those given for the data in Fig. 3; however, the convective Mach number was equal to 1.5, the convective velocity was approximately 3000 ft/sec, and the dynamic pressure was 325 psia. Unlike the photographs of Fig. 3, the liquid removed from the surface under these flow conditions converges into a wake having a triangular shape.

An analysis of the shapes of the windward surfaces of all of the various droplets photographed indicated that the droplets were deformed into ellipitical shapes as shown, for example, in Fig. 5. The diagram comprising Fig. 5 is taken directly from the enlarged photograph shown in Fig. 4. The shaded portion in the figure represents the volume which the original droplet mass would occupy assuming that the deformed droplet shape is a planetary ellipsoid having a planar leeward surface. The eccentricity of the ellipse changed as the drop was accelerated.

Some of the data obtained from the image converter pictures, such as those shown in Figs. 3 and 4, is displayed in Figs. 6 and 7. Figure 6 shows the variation of the normalized drop diameter plotted against the dimensionless time while Fig. 7 gives the dimensionless displacement history. The dimensionless time parameter $\overline{T}$ originated from an analysis presented in Ref. 2. These figures demonstrate quite clearly that both the deformation and the acceleration histories of both large and small droplets subjected to widely diverse aerodynamic conditions exhibit a striking dynamic similarity when cast in these dimensionless terms. Complete droplet breakup is indicated when $4 \leq \overline{T} \leq 5.5$ thus giving a dimensionless breakup distance $20 \leq \overline{x} \leq 30$.

Determinations of the shape of the windward face of the drop from the image converter photographs along with conservation of mass suggests that the drop shape may change in manner shown in Fig. 8.

A sample of the type of data which was gathered with the rotating drum camera is shown in Figs. 9, 10, 11, 12, 13, and 14. The streak photographs which were obtained, such as those shown in Figs. 9 and 11, were extremely useful because of the enormous amount of information that each one provided. For example, Fig. 9 and 11 show the shattering of an 1100μ droplet when $P_1 = 1$ atmos., $U_2 = 800$ ft/sec, $M_2 = 0.65$, $q_2 = 10$ psia, and $P_1 = 1$ atmos., $U_2 = 1980$ ft/sec, $M_2 = 1.2$, and $q_2 = 110$ psia, respectively. Since a 0.125 in. wide slit was used, the shock front appears to be unusually thick. The lines extending the length of the photographs are images of the vertical fiducial markers which were placed one inch apart on the test section windows.

These streak photographs clearly demonstrate the continuous nature of the shattering process under both subsonic and supersonic flow conditions. Each photograph reveals that the displacement traced out from the motion of the shadow cast by the forward stagnation point is a smooth, continuously varying function of time. In other words, no abrupt changes in the local shape of the displacement curves are visible. On the basis of these observations, it seems reasonable to conclude that both the droplet mass and frontal area are also smooth functions of time; otherwise, one might expect to observe discontinuities in the shape of the displacement curve. The results of these experiments, therefore, do not completely confirm those of Nicholson[5] who reported a discontinuity in his displacement data which was interpreted as a sudden increase in droplet acceleration and defined as the breakup time. Since Nicholson used a Fastax camera whose interframe time was 80 μsec, his displacement data suffered from a lack of good time resolution which may explain the interpretation of the results.

Tracings of the streak photographs are presented in Figs. 10 and 12 to show the displacement (x) and time (t) scales, and to identify the particle path, the drop trajectory, and the point (χ, τ) at which the local slope of the displacement curve is equal to 95% of the convective flow velocity, U_2, behind the shock front. The important influence of the dynamic pressure on the rate at which the shattering occurs can be appreciated by comparing these two figures. For example, in Fig. 10 where q_2 = 10 psia, the stripping process is seen to begin at approximately 50 μsec and the drop is accelerated to a velocity equal to 0.95 U_2 within a period of about 700 μsec. In Fig. 12 where q_2 = 110 psia, stripping is observed to begin within several microseconds after contact with the shock and the drop is accelerated to a velocity equal to 0.95 U_2 within a time slightly less than 300 μsec. It is of interest to note that, in both the subsonic and supersonic cases, the material which is initially removed from the drop surface is accelerated almost instantaneously to the particle velocity behind the wave front, thus giving additional evidence of the small size of these particles. For example, assuming that the tiny particles are spherical with C_D = 1-3, then their size, calculated using data from Fig. 12, is found to be approximately 10-2μ, respectively.

A number of experiments were run with drop sizes 1000-4000μ in diameter spread over a Mach number range of M_S = 1.5-5.7. Some typical displacement results obtained from the streak photographs are shown in Fig. 13. The points at which the local slopes of the displacement curves are equal to 0.95 U_2 are designated as (χ, τ). Referring to Fig. 13, one observes that the characteristic time τ decreases from a value of about 560 μsec for M_S = 1.52 to a value of approximately 170 μsec at M_S = 3.21 for the different indicated drop sizes. The corresponding characteristic distance X varies from about 2 in. to 3.2 in. It is interesting to note that if $\bar{\chi}(= \chi/D_o)$ is calculated it is found to have a constant value approximately equal to $\bar{\chi} \approx 50$. This is a rather surprising result when one considers the wide range of conditions for which it is valid. In other words, over an extremely broad range of drop size and dynamic pressure conditions, the distance a disintegrating drop travels while being accelerated up to 0.95 U_2 is a constant and approximately equal to X ≈ 50 D_o.

If these curves are replotted in terms of the dimensionless coordinates $(\bar{X}, \bar{T})$, then we obtain the results shown in Fig. 14. One observes that the data collapse into a system of similarity curves which appear to have some parametric dependence on the convective flow Mach number. For example, setting $\bar{X} = \bar{\chi} = 50$, the corresponding values of $\bar{T}$ range from about 6 to 7.5 depending on the value of M_2. An adequate physical explanation for the effect of the Mach number on the displacement is complicated by the complex nature of the shattering phenomenon. Not only is the drop shape changing rapidly with time, thus altering the external pressure field around it, but the surface is being simultaneously stripped away which consequently reduces its mass. The coupled effects, therefore, of a changing drag and a diminishing mass are manifest in the non-dimensional displacement history, and any hope of being able to separate the two, for the purpose of giving a satisfactory rational explanation for the Mach number effect, seems very slight indeed.

A comparison of the streak and image converter data leads to several important conclusions regarding the definition of a quantitative breakup criterion. For example, two different sets of streak and image converter displacement data are shown and compared in Fig. 15. Since all of the parameters are constant except the initial droplet diameters, the differences between these two sets of data are due entirely to an effect of drop size. As one would expect, the small drop possesses less inertia and, hence, it accelerates more rapidly than the larger one. Furthermore, the breakup time (t_b) of the small drop is approximately one-half that of the large one. Since the two diameters differ by a factor of two, we conclude that $t_b \sim D_o$. The agreement between the individual data points and the streaked displacement appears to be rather good, thus indicating that the technique of finding the displacement from individual photographs can be employed with reasonable accuracy.

Referring again to Fig. 15, it is interesting to observe that the local slope of the streak curves, in the neighborhood of t_b, is approximately equal to 0.60 U_2. In other words, by the time the droplets have been accelerated to a speed approximately equal to 60% of the convective flow velocity, they are completely disintegrated. By applying this quantitative breakup criterion to the streak data, the corresponding dimensionless breakup times ($\overline{T}_b$) and distances ($\overline{X}_b$) can be calculated and compared with those found from the image converter data. The two dimensionless breakup times are plotted in Fig. 16 as a function of the convective flow Mach number for a variety of aerodynamic conditions corresponding to a Reynolds number range of $13,500 \leq Re \leq 413,000$ and a Weber number range of $695 \leq We \leq 85,500$. The indication is that the two sets of data agree quite well with one another both in magnitude and in distribution with M_2. The apparent shape of the $\overline{T}_b$ distribution is strikingly similar to the drag coefficient curve for a spherical body, however, this may be just a coincidence and have no real physical significance. The conclusion to be drawn from Fig. 16 is that the dimensionless breakup time is relatively constant, $\overline{T}_b \approx 5$, over a wide range of drop size and aerodynamic conditions. However, there is some indication to suggest that its value should be slightly lower when $M_2 < 1$ and a bit higher when $M_2 \geq 1$.

The corresponding dimensionless distances are plotted versus M_2 in Fig. 17 where one notes from the variation that $\overline{X}_b$ is approximately a constant except at the subsonic end of the distribution where it falls off somewhat from the mean value of $\overline{X}_b \approx 25$.

4. CONCLUSIONS

The results of the study presented here indicate that the impact by a strong shock wave is an insignificant element in producing the aerodynamic shattering of liquid drops. The main function of the shock is to produce the high speed convective flow which is responsible for the ensuing disintegration. Under the conditions of high dynamic pressure, breakup begins almost instantaneously following interaction with a shock front. A drop which is originally spherical is deformed into a planetary ellipsoid with its major axis perpendicular to the direction of the flow. The shearing action exerted by the high speed flow causes a boundary layer to be formed in the surface of the liquid. These studies further support the fact that the breakup time is proportional to the drop diameter, inversely proportional to the velocity, and proportional to the square root of the liquid to gas density ratio, and they reveal a secondary Mach number effect on the breakup time and distance.

NOMENCLATURE

a_1 = speed of sound in driven section

a_2 = speed of sound in convective flow

C_D = drag coefficient

D_o = initial droplet diameter

M_S = incident shock Mach number ($= U_S/a_1$)

M_2 = convective flow Mach number ($= U_2/a_2$)

P_1 = driven section initial pressure

q_2 = convective flow dynamic pressure ($= 1/2\ \rho_2 U_2^2$)

Re = Reynolds number ($= \rho_2 U_2 D_o/\mu_2$)

t = time

t_b = breakup time; time to accelerate to 0.6 U_2

$\bar{T}$ = dimensionless time ($= [U_2/D_o][\rho_2/\rho_\ell]^{1/2} t$)

$\bar{T}_b$ = dimensionless breakup time ($= [U_2/D_o][\rho_2/\rho_\ell]^{1/2} t_b$)

U_S = incident shock velocity

U_2 = convective flow velocity

W_e = Weber number ($= \rho_2 U_2 D_o/\sigma$)

x = displacement

$\bar{X}$ = dimensionless displacement ($= x/D_o$)

μ_2 = convective flow viscosity coefficient

ρ_2 = convective flow density

ρ_ℓ = droplet density

σ = droplet surface tension

τ = time when droplet velocity = 0.95 U_2

$\bar{\tau}$ = dimensionless time ($= [U_2/D_o][\rho_2/\rho_\ell]^{1/2}\tau$)

χ = displacement when droplet velocity = 0.95 U_2

$\bar{\chi}$ = dimensionless displacement ($= \chi/D_o$)

REFERENCES

1. Dabora, E. K., Ragland, K. W., and Ranger, A. A., "Two Phase Detonations and Drop Shattering Studies," Second Annual Progress Report. 06324-2-T, April 1966, University of Michigan, Ann Arbor, Michigan.

2. Ranger, A. A., and Nicholls, J. A., "Aerodynamic Shattering of Liquid Drops," AIAA Journal, Vol. 7, No. 2, February 1969.

3. Ranger, A. A., "The Aerodynamic Shattering of Liquid Drops," Ph.D. Dissertation, The University of Michigan, 1968.

4. Engel, O. G., "Fragmentation of Waterdrops in the Zone Behind an Air Shock," Journal of Research of the National Bureau of Standards, Vol. 60, No. 3, March 1958.

5. Nicholson, J. E., and Hill, A. F., "Rain Erosion on Spike Protected Supersonic Radomes," MC-61-R3, April 1965, Mithras Inc., Cambridge, Massachusetts.

6. Reinecke, W. G., and McKay, W. L., "Experiments on Water Drop Breakup Behind Mach 3 to 12 Shocks," SANDIA Laboratories, SC-CR-70-6063, Albuquerque, New Mexico, June 1969.

7. Dabora, E. K., "Production of Monodisperse Sprays," Review of Scientific Instruments, Vol. 38, April 1967, pp. 502-506.

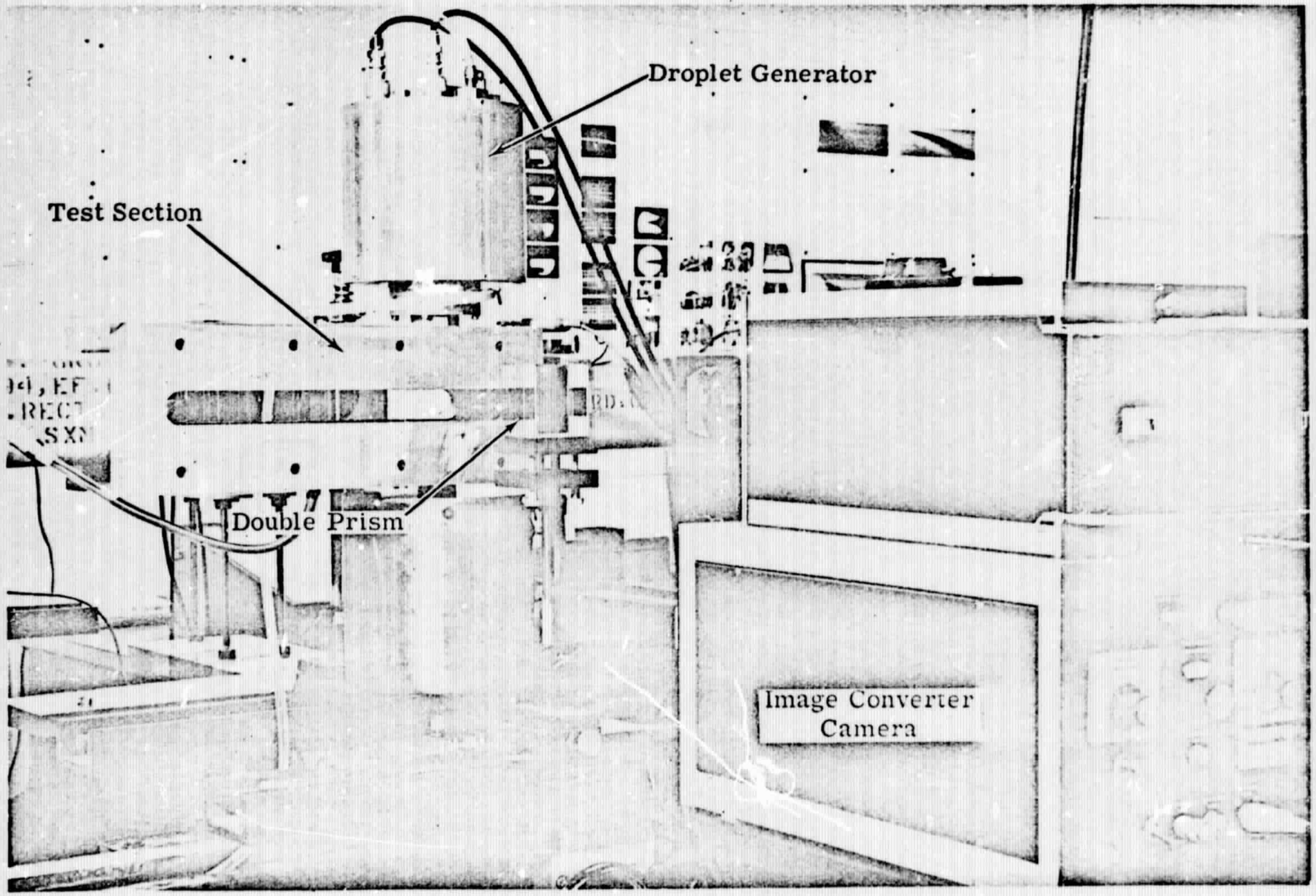

Fig. 1 Shock Tube Test Section.

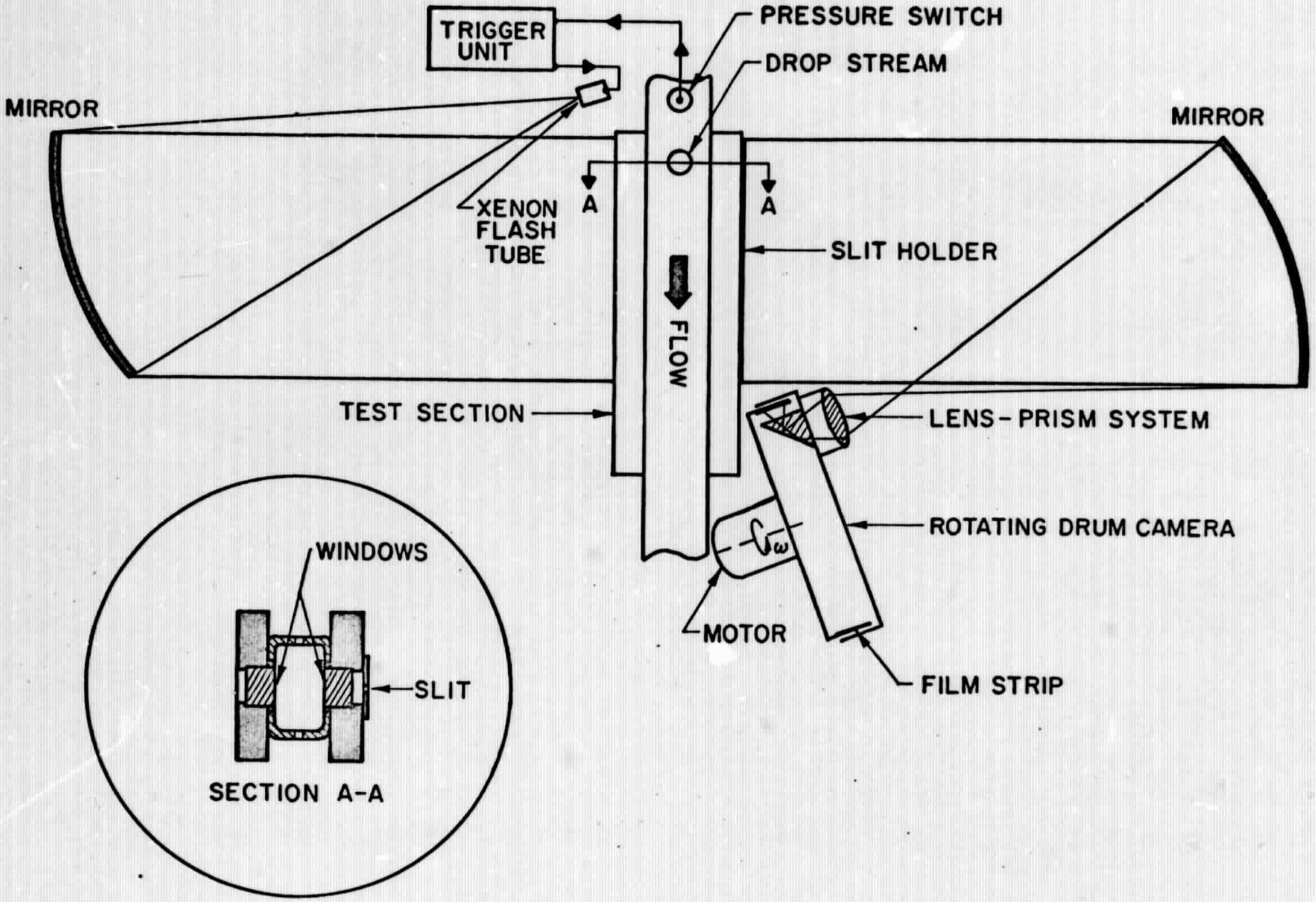

Fig. 2 Rotating Drum Camera Arrangement.

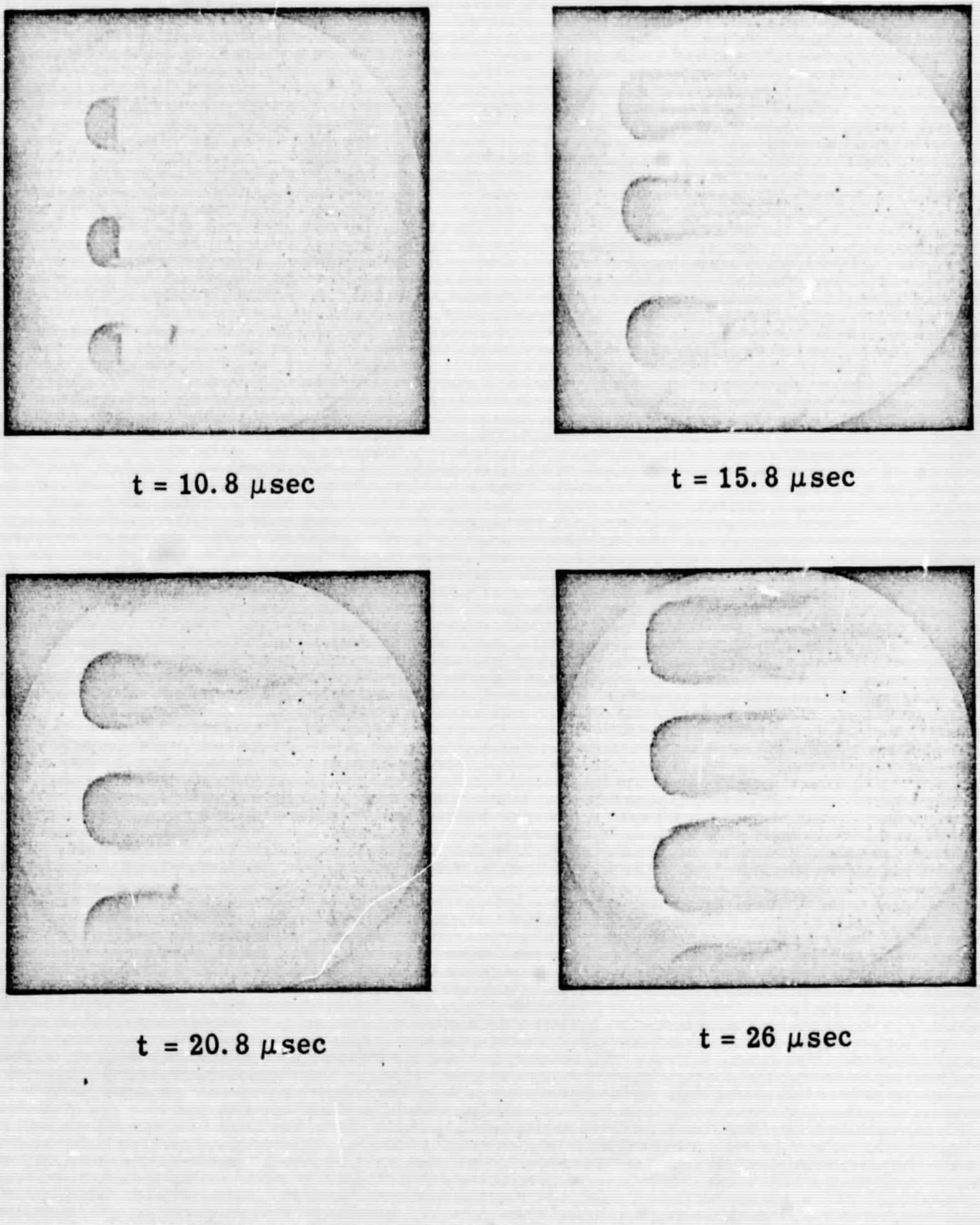

t = 10.8 μsec

t = 15.8 μsec

t = 20.8 μsec

t = 26 μsec

Fig. 3 (cont.) Shattering of 750μ Droplets when M_s = 2.0.

Fig. 4 Shattering of 2700μ Droplet when M_s = 3.5, t = 14 μsec.

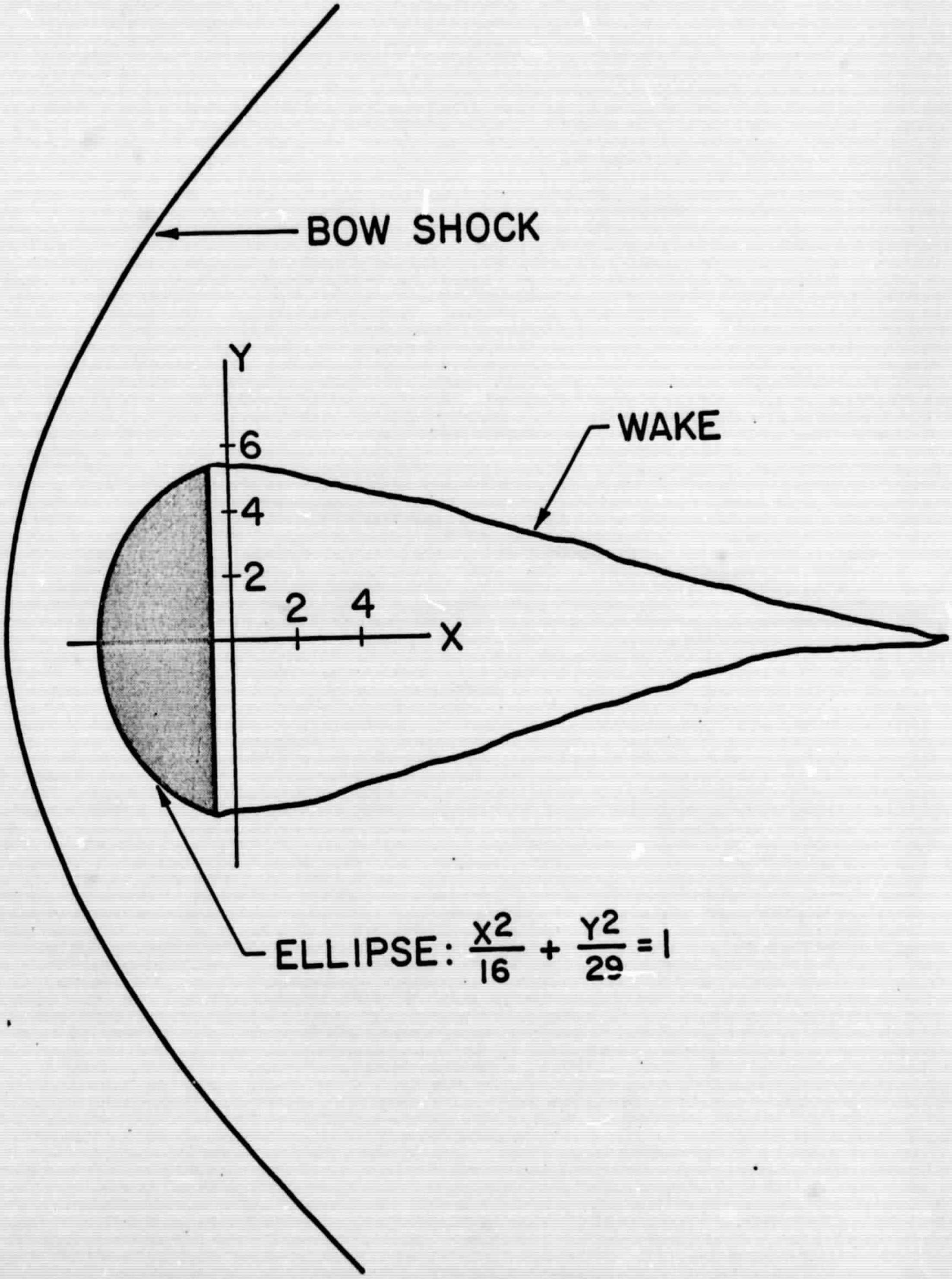

Fig. 5 Droplet Shape.

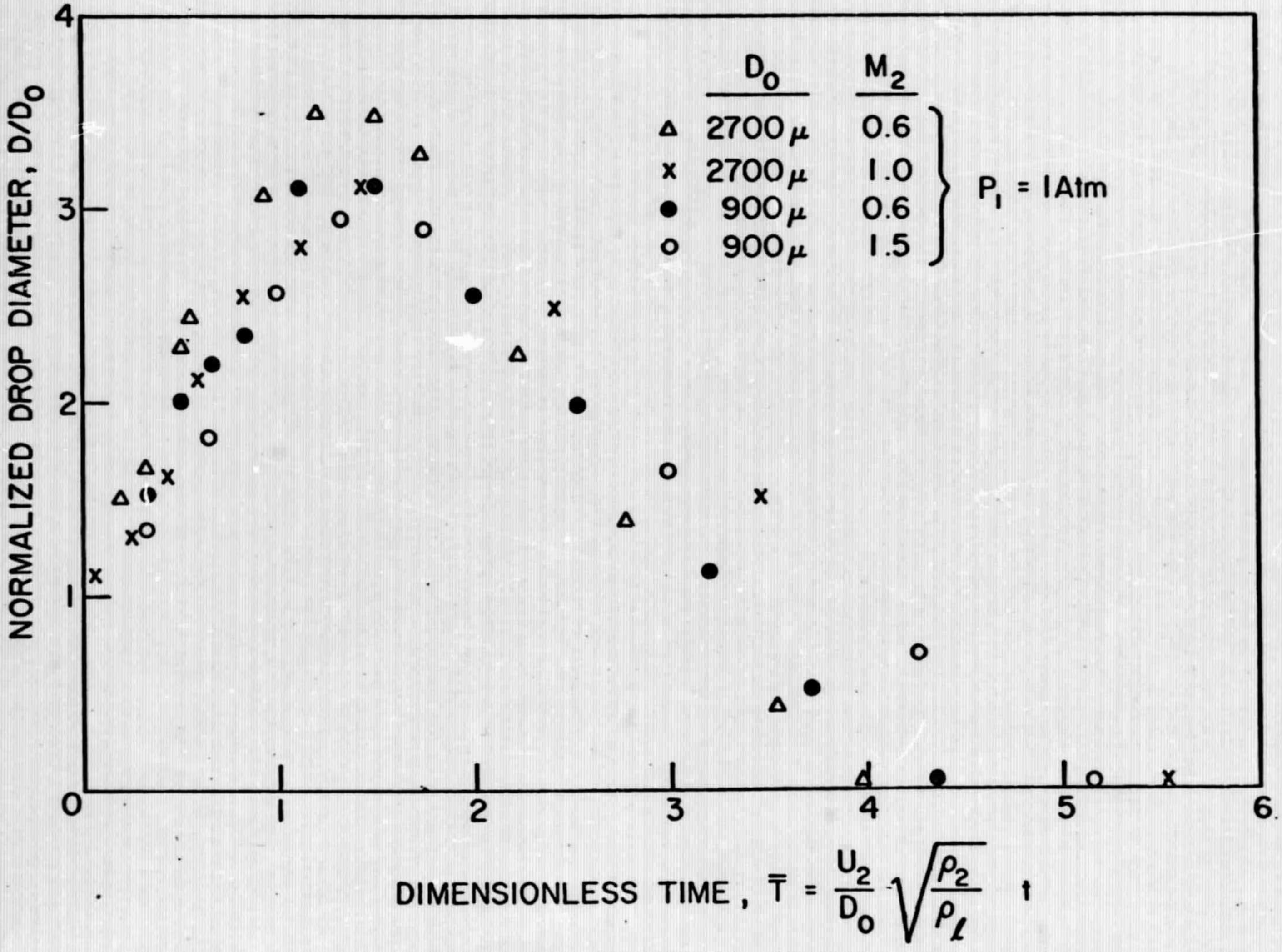

Fig. 6 Variation of Dimensionless Diameter with Dimensionless Time.

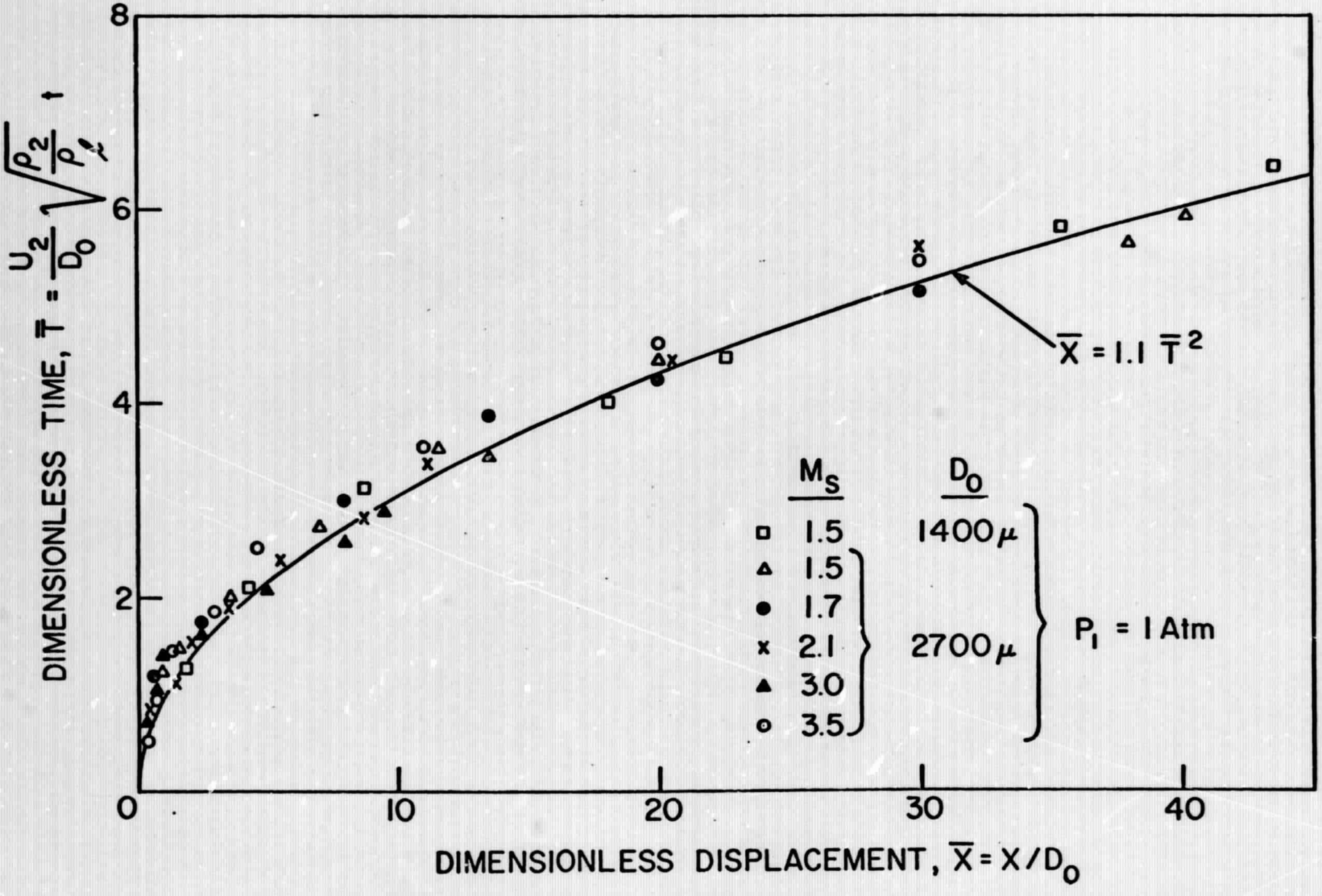

Fig. 7 Variation of Dimensionless Displacement with Dimensionless Time.

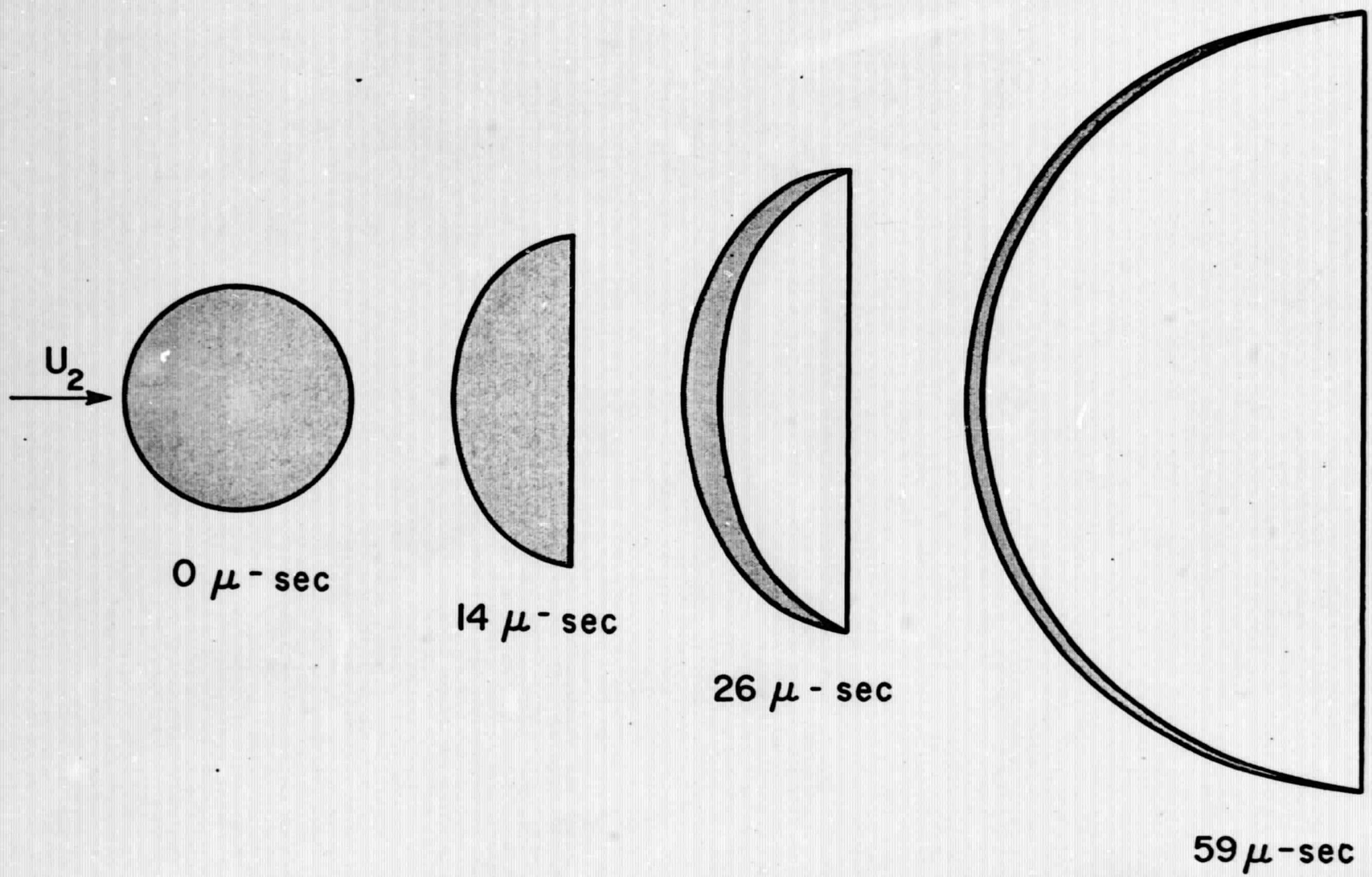

Fig. 8

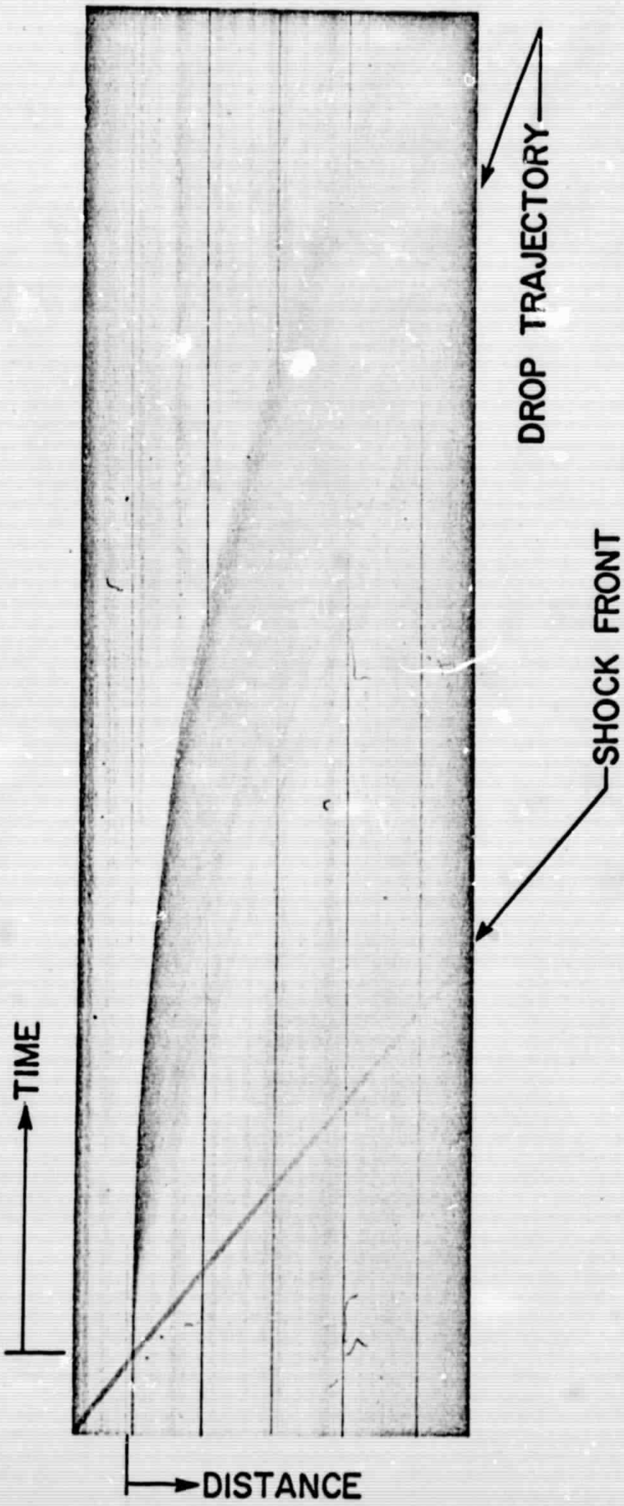

Fig. 9 Shattering of 1100μ Droplet when M_s = 1.6.

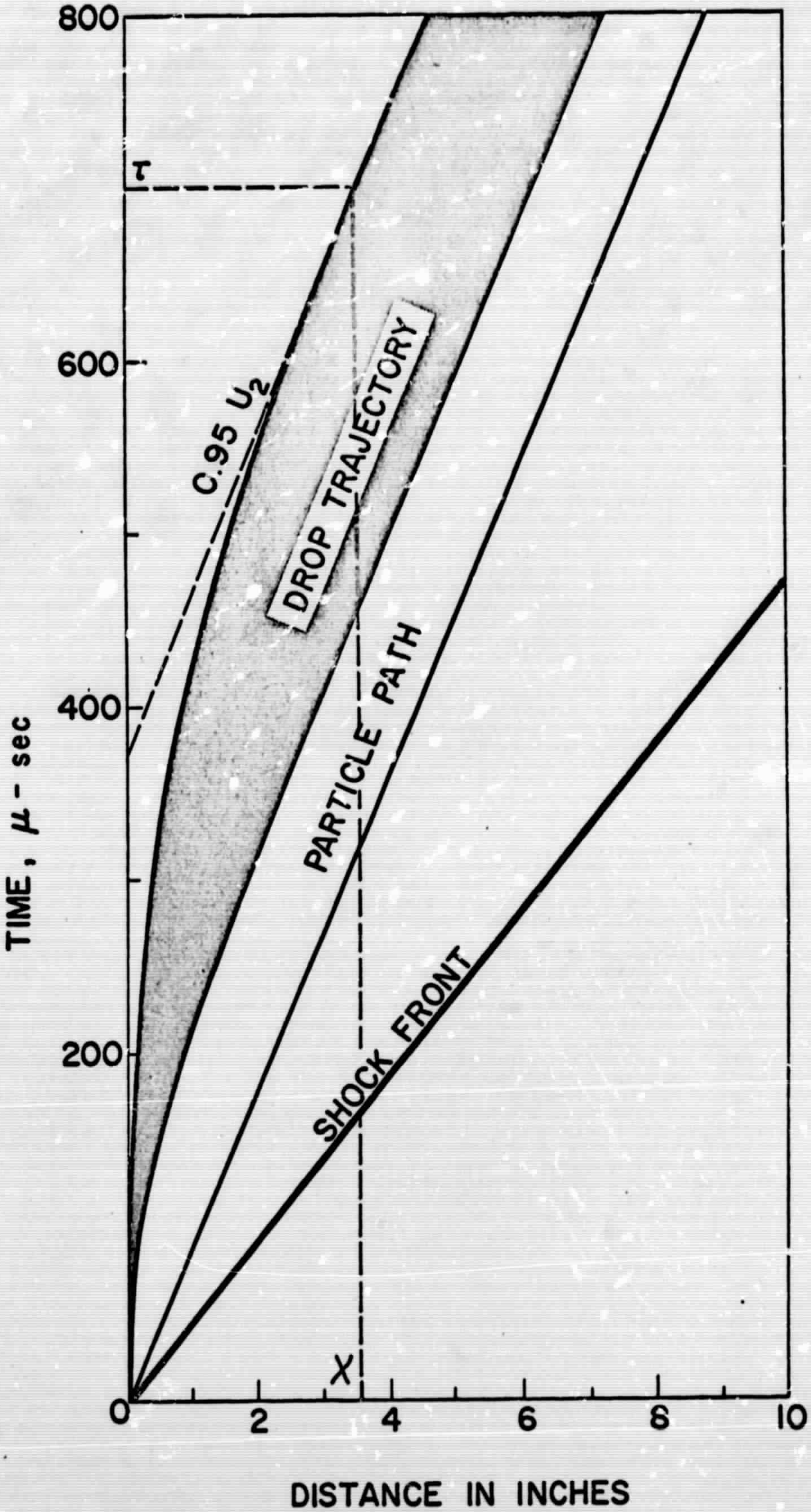

Fig. 10 Shattering of 1100μ Droplet when M_s = 1.6.

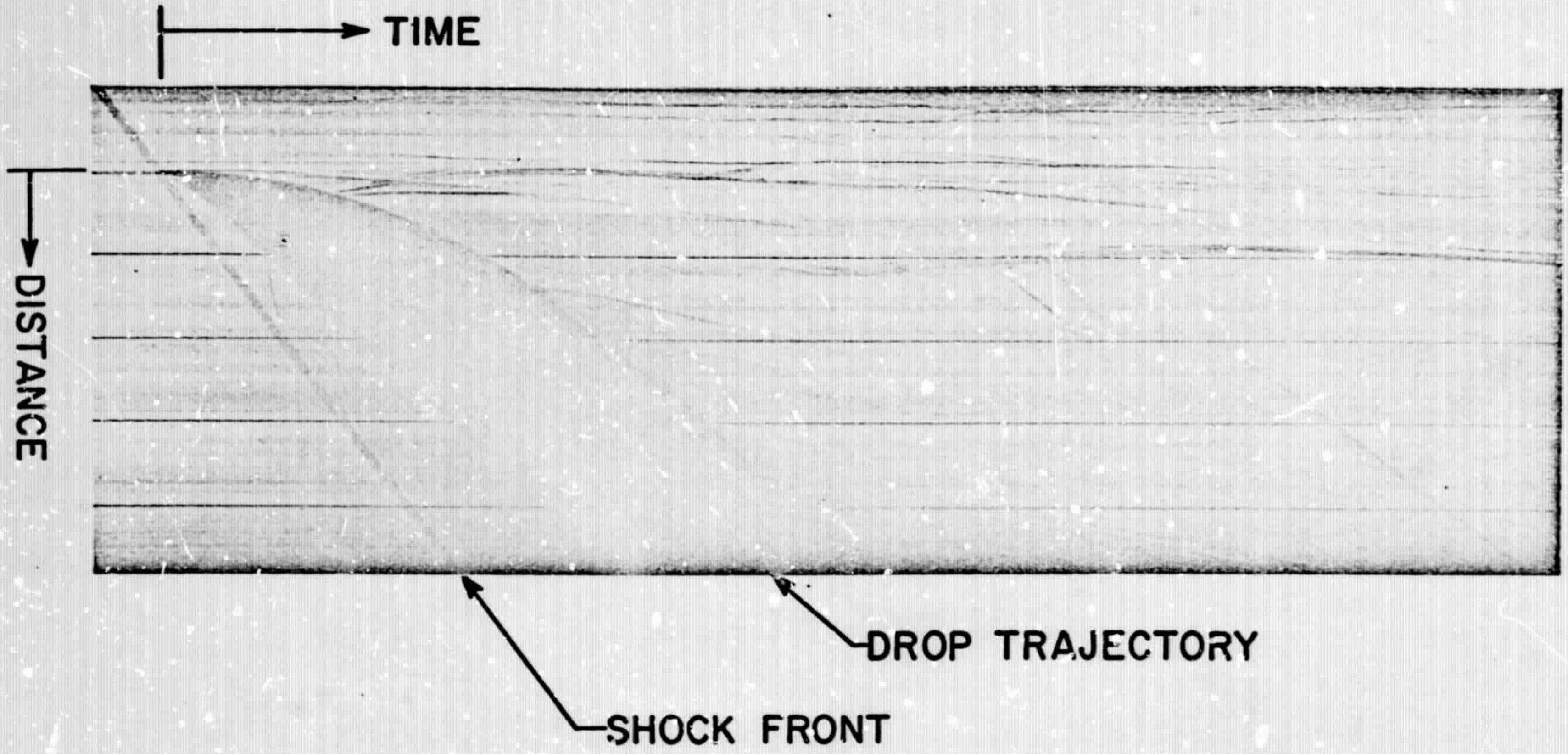

Fig. 11 Shattering of 1100μ Droplet when $M_s = 2.5$.

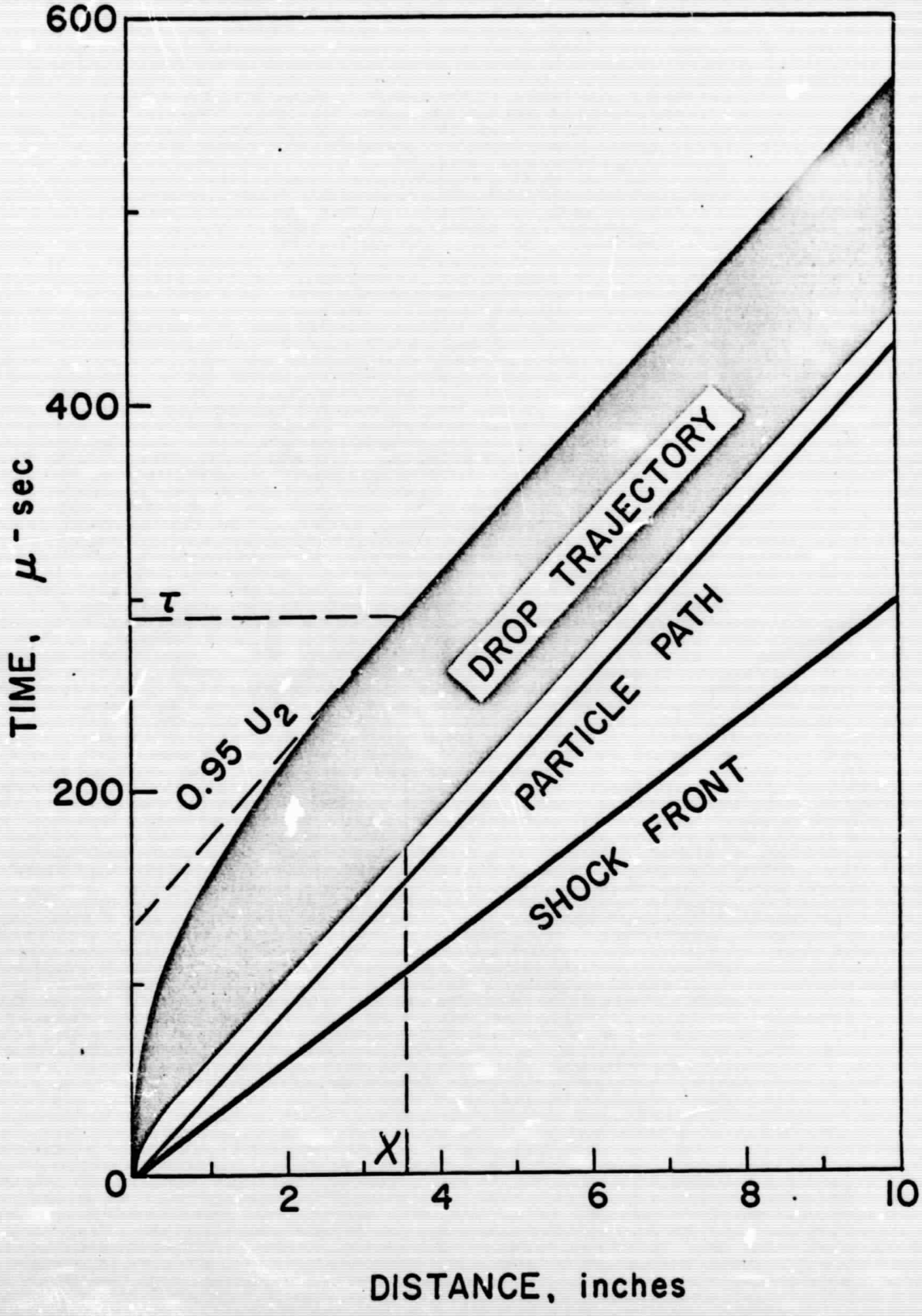

Fig. 12 Shattering of 1100μ Droplet when $M_s = 2.5$.

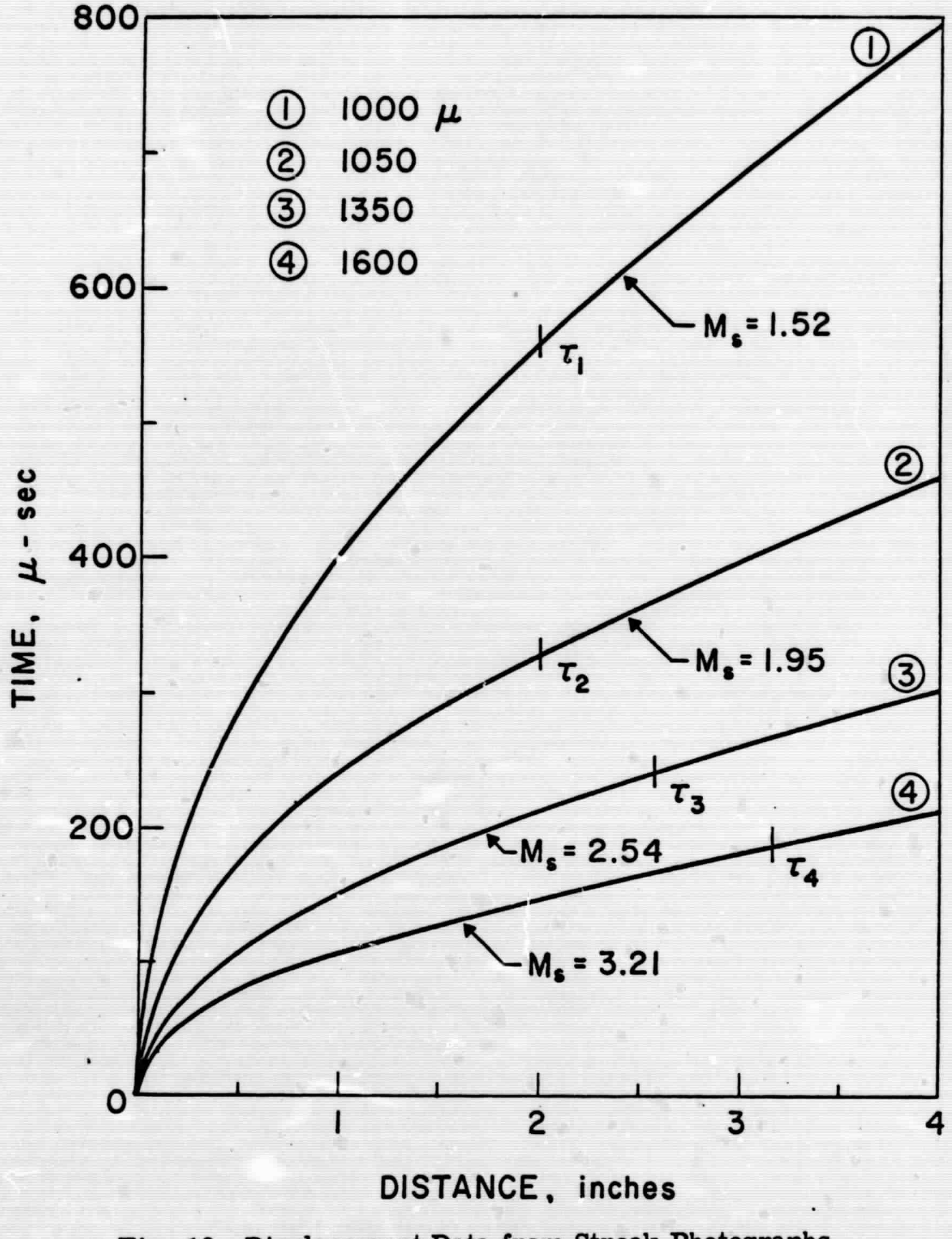

Fig. 13 Displacement Data from Streak Photographs.

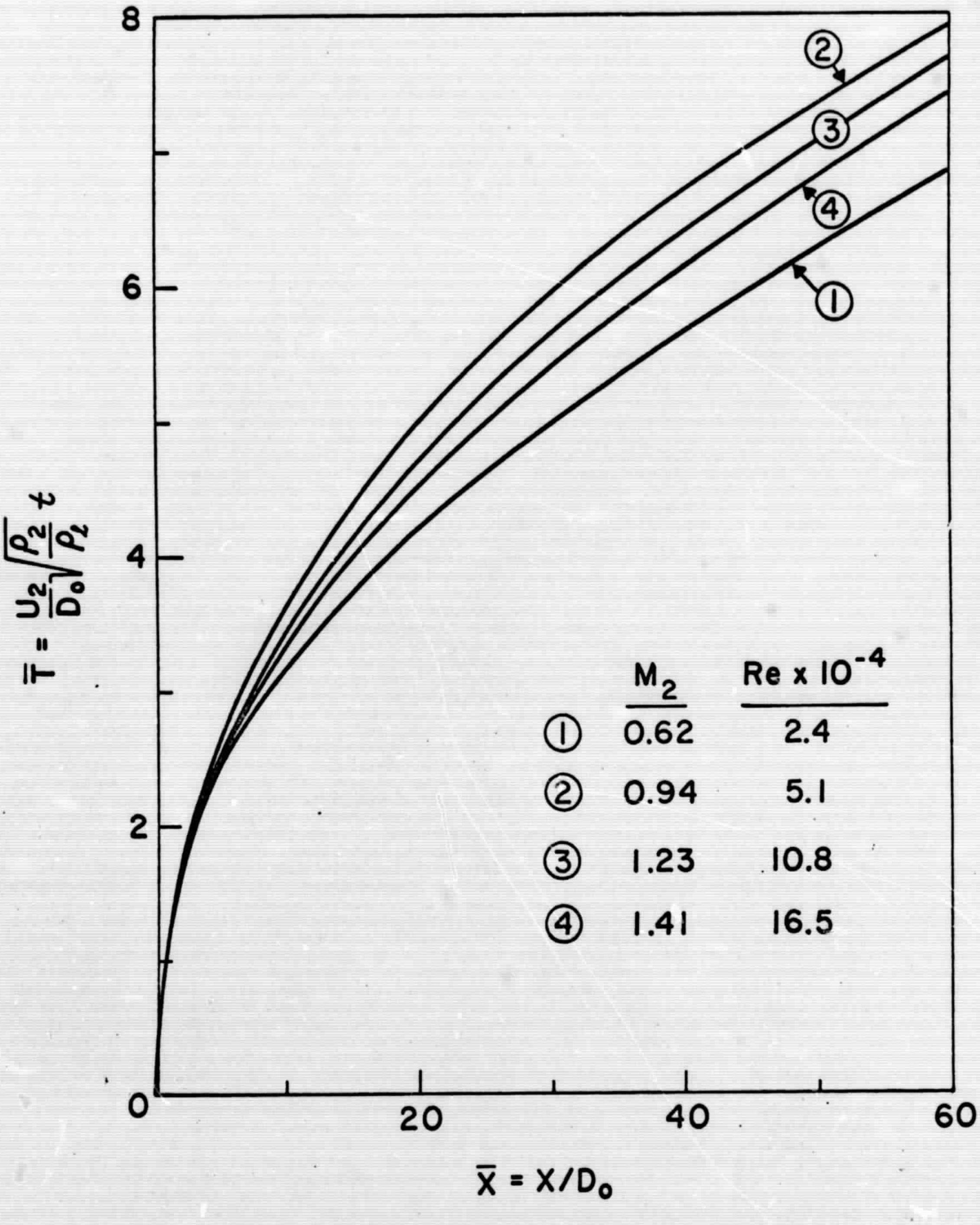

Fig. 14 Dimensionless Displacement.

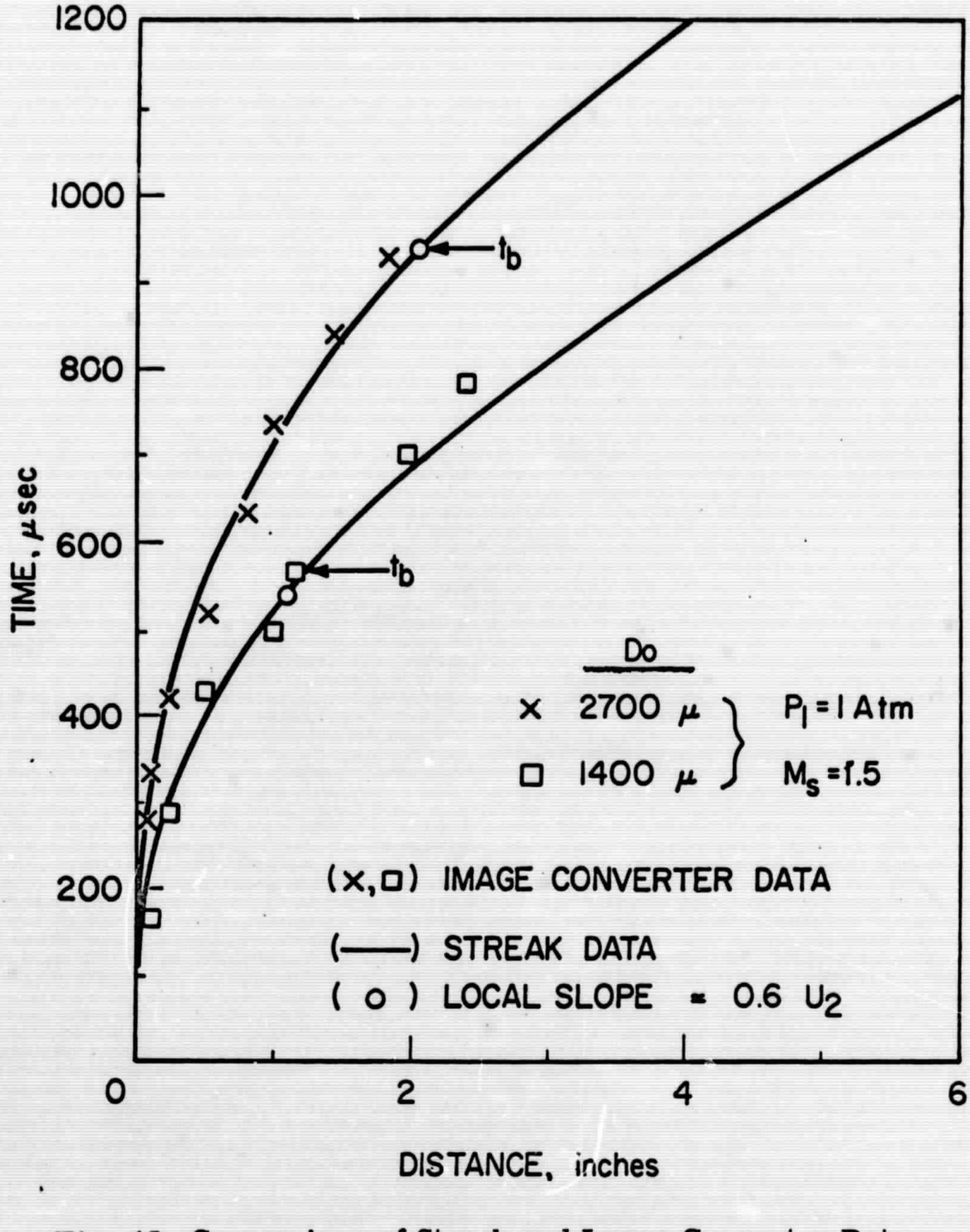

Fig. 15 Comparison of Streak and Image Converter Data.

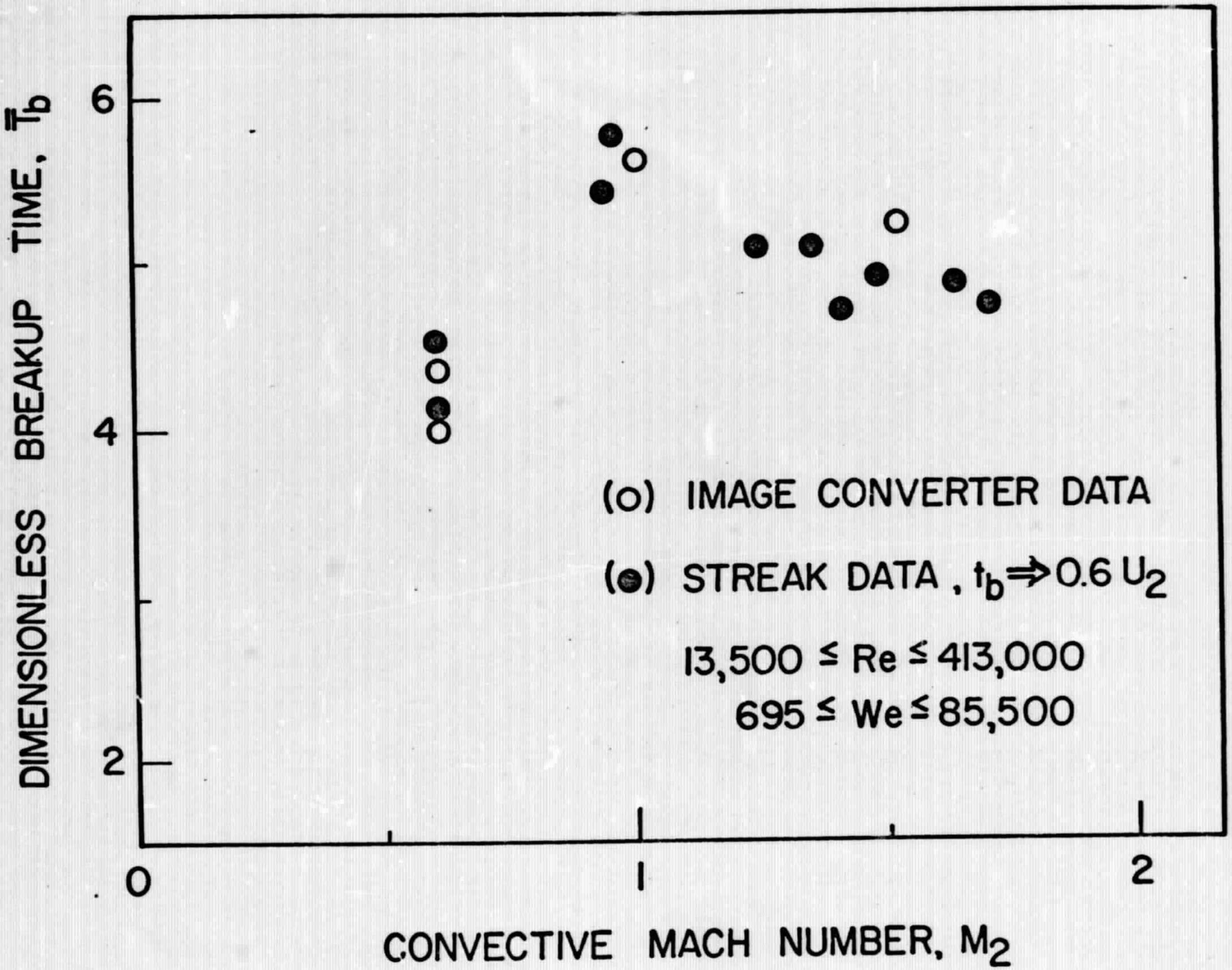

Fig. 16 Comparison of Dimensionless Breakup Times.

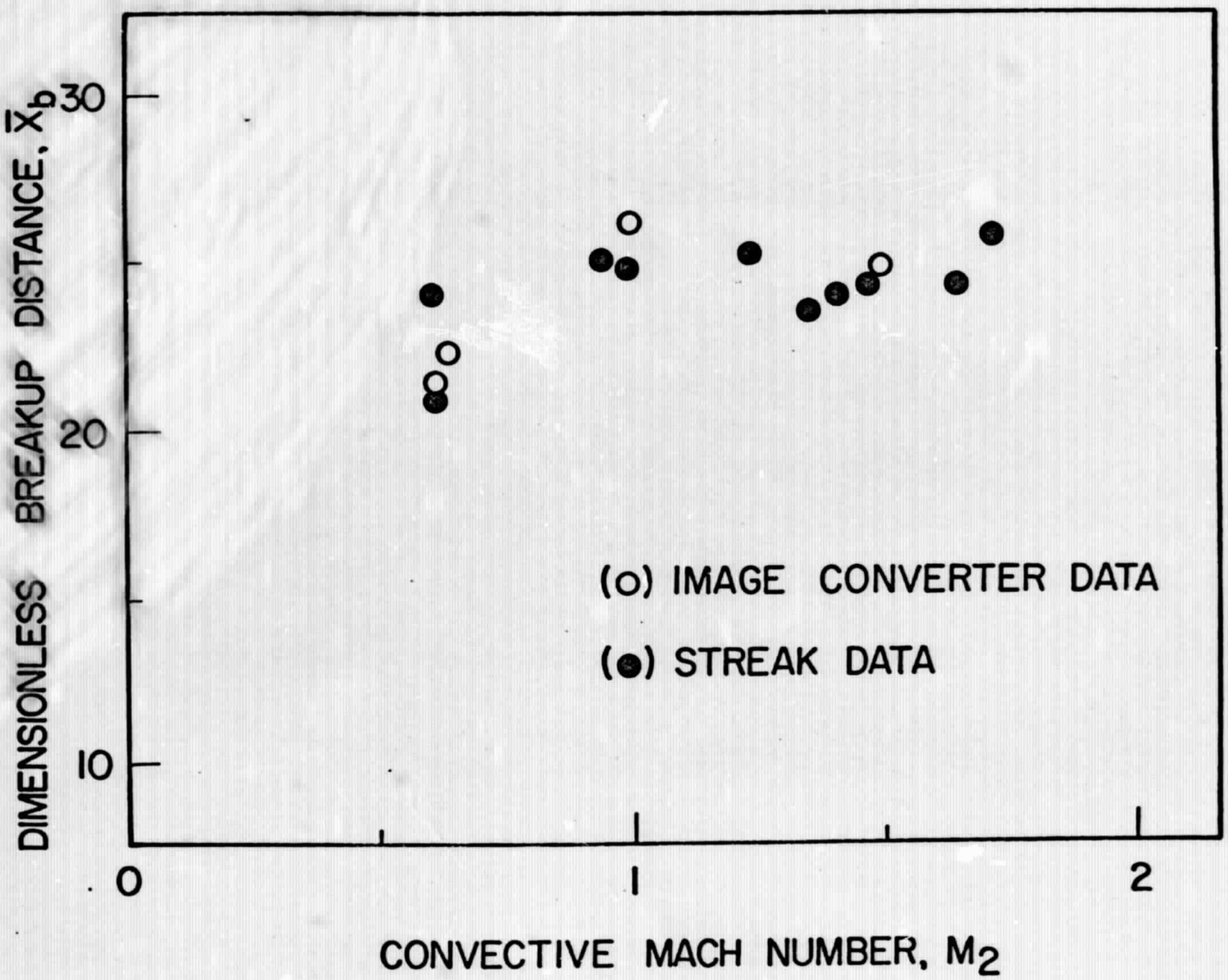

Fig. 17 Dimensionless Breakup Distance.

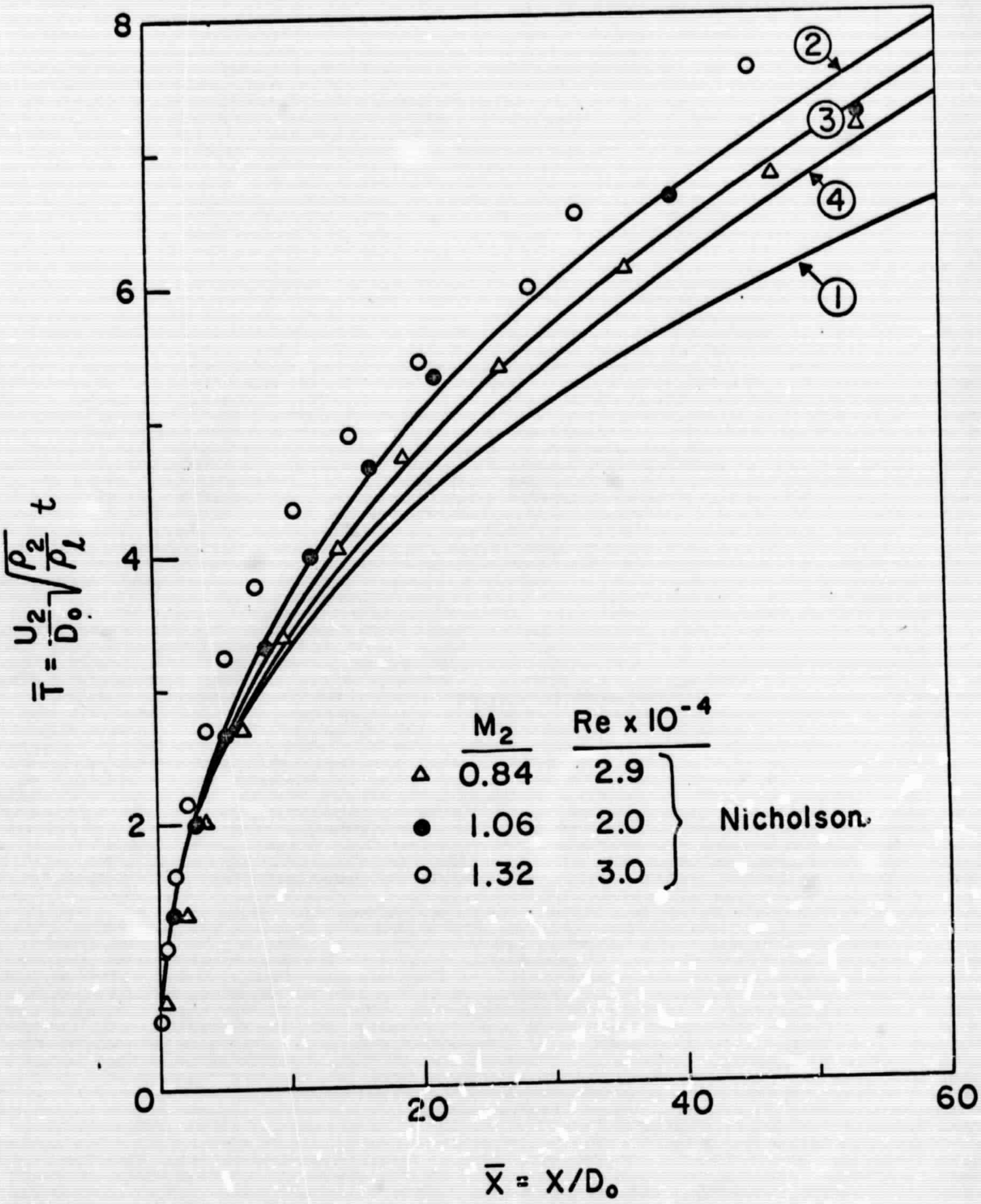

Fig. 18 Comparison of Dimensionless Displacement with the Present Study.